A 18-ms Measurement-Time MLS-Based System for Moisture Assessment in Lubricant Oil

Antonio Vincenzo Radogna, *Member, IEEE*, Chiara De Pascali, Elisa Sciurti, Maria Assunta Signore, Stefano D'Amico, *Senior Member, IEEE*, and Luca Francioso

***Abstract*— In this article, a system and a measurement approach to reduce the measurement time in the assessment of moisture contamination in lubricant oils is presented. The system's sensing principle leverages the permittivity change of a miniaturized interdigital capacitor (IDC) while immersed in oil. The time-domain impedance concept, that is, the impulse response (IR), is exploited by using maximum length sequences (MLSs) as efficient broadband signals for the sensor's excitation in a wide range of frequencies. Different from conventional impedance spectroscopy (IS), MLS-based measurements are performed with simpler hardware, higher computational efficiency, lower power consumption, and lower measurement time. As a novelty with respect to the state-of-the-art, this article introduces a linear model to relate a single measured quantity from the IR to water concentration in oil. This permits to reduce the digital processing operations, leading to low measurement time and, thus, to low energy-per-measurement parameters with respect to other works which rely on laboratory instrumentation. The validity of the linear model, for the detection of small concentrations of water in lubricant oil, has been verified through experimental measurements. Water–oil samples have been prepared with 0.2 vol%, 0.5 vol%, 1 vol%, 2 vol%, and 3 vol% water concentrations at room temperature, obtaining an estimated limit of detection (LOD) of 6.3 ppm. A low measurement time of 18 ms has been achieved which advances the state-of-the-art.**

***Index Terms*— Fast impedance measurement, industrial fluid, interdigital capacitive sensor, lubricating engine oil, moisture detection.**

I. Introduction

LUBRICANT oils are commonly adopted for the maintenance and correct operation of engines and machinery in general. Basically, they provide a protective film aimed at the reduction of the contact between the moving components of the engine and, thus, minimizing the effect of friction [1], [2]. As a result, the overheating and wear of parts are minimized during the functioning, guaranteeing high longevity of machinery. Additional key features of lubricant oils include the cooling of parts, sealing of clearances, and protection against corrosion and potential occlusions. During the engine's normal operation, the oil absorbs contaminants due to aging or accidental contamination of external substances [3], leading to physical and chemical degradation of its composition. Water is one of the major contaminants of lubricating oil [4], [5], resulting to be detrimental to the lubricant properties of oil and causing corrosion and accelerating oil oxidation [6]. Fast and accurate monitoring of water contamination in lubricants is mandatory to predict the oil's health status, thus permitting a prompt replacement. This offers a twofold benefit: the correct maintenance of engines is guaranteed, and the costs and waste of unnecessary oil replacements are minimized [3]. Moreover, the knowledge of the water concentration can be useful for the determination of the water activity and the relative saturation of the lubricant oil. The first is obtained by experimental determination of the moisture sorption isotherm curve. The latter is obtained by experimental measurement of the water-in-oil solubility at the working temperature.

In a typical application, offline laboratory analyses are carried out every few months [7] to determine the health status of the lubricant. In most cases, the low sampling rate of analysis results is inadequate for a proper prognostic of the engine's health, thus preferring the more frequent inline monitoring approach [6].

The literature provides many examples of inline devices for monitoring lubricant oils' contamination. In [6], a sensor based on an electrical resonant circuit has been developed. Thanks to four output variables, the sensor can predict, through laboratory instrumentation measurements and subsequent principal component analysis (PCA), various parameters such as moisture concentration, aging, and total acid number (TAN). The measurement is performed by a network analyzer at tens of megahertz, obtaining a limit of detection (LOD) of 1 ppm with a minimum water concentration of 25 ppm. An alternative approach is proposed in [4] where 2.25 MHz ultrasonic waves, along with artificial neural networks, have been exploited for moisture assessment in oil samples. An average error of 11.3% is obtained for the assessment with a minimum tested water concentration of 0.1%. The cited works rely on laboratory instruments to perform the

Manuscript received 16 February 2023; revised 13 June 2023; accepted 19 June 2023. Date of publication 3 July 2023; date of current version 17 July 2023. This work was supported by the SMEA PON Project (Diagnostic and Prognostic Methods and Sensors Development for the Health Monitoring in Aeronautic and Transport applications), Grant number (CUP): B84G14000070005. The Associate Editor coordinating the review process was Dr. Guanfeng Du. *(Corresponding author: Chiara De Pascali.)*

Antonio Vincenzo Radogna is with the Institute for Microelectronics and Microsystems (IMM), National Research Council (CNR), 73100 Lecce, Italy, and also with the Department of Engineering for Innovation, University of Salento, 73100 Lecce, Italy (e-mail: antonio.radogna@imm.cnr.it).

Chiara De Pascali, Elisa Sciurti, Maria Assunta Signore, and Luca Francioso are with the Institute for Microelectronics and Microsystems (IMM), National Research Council (CNR), 73100 Lecce, Italy (e-mail: chiara.depascali@cnr.it; elisa.sciurti@imm.cnr.it; mariaassunta.signore@cnr.it; lucanunzio.francioso@cnr.it).

Stefano D'Amico is with the Department of Engineering for Innovation, University of Salento, 73100 Lecce, Italy (e-mail: stefano.damico@unisalento.it).

Digital Object Identifier 10.1109/TIM.2023.3291775

measurements which are typically heavy, large in size, power-hungry, and require a connection with a personal computer for data processing and display. Differently, the solution proposed in [5] combines a miniaturized interdigital capacitor (IDC) with a commercial integrated impedance analyzer, that is, the AD5933. This solution leverages impedance measurements to assess the moisture contamination through changes in the dielectric constant of the IDC, obtaining an accuracy of 98.6% with a minimum tested water concentration of 0.05%. Although the latter system shows interesting features, such as miniaturization, portability, and lower power consumption with respect to laboratory-based solutions, it relies upon the conventional impedance spectroscopy (IS) approach which is also adopted by most of the works in literature. The IS uses narrowband signals, that is, single-tone sinusoids, as excitation signals for the system under test, which severely limits the measurement time for the impedance read-out. The reason is that it depends on the minimum frequency point used for the excitation. As a result, the energy-per-measurement parameter, which must be low to use the device with a battery-powered supply, is increased. Moreover, accurate IS measurements require a design effort on both analog and digital hardware to implement proper sensor interfacing, excitation, read-out, and signal processing [8].

In this article, a system and a measurement approach to dramatically reduce the measurement time in the assessment of moisture contamination in lubricant oils is presented. This approach is suitable for the inline implementation of monitoring systems for the assessment of lubricant oils' health conditions. The time-domain impedance concept, that is, the impulse response (IR), is exploited by using maximum length sequences (MLSs) as excitation signals for the sensor. Differently from narrowband signals, MLSs are broadband, permitting to excite the sensor in a wide range of frequencies with a single signal [9], [10], [11], [12]. Differently from [13], which thoroughly presents the theoretical foundations of MLS-based measurement with simulated discrete-component sensors, this article adopts the MLS-based approach in a practical application with a real capacitive sensor. Moreover, the proposed method aims to relate the information on water contamination in lubricant oil samples to a single measured point. This is in contrast with conventional IS systems. Indeed, the latter requires multifrequency excitation along with a postprocessing for fitting the measured impedance in sensors' electrical models. These advantages permit achieving, besides a low hardware and firmware effort for the development, also a low-power operation and a low measurement time. These are needed to keep a low energy-per-measurement, thus allowing the adoption of the proposed system in battery-powered inline monitoring devices for adoption in smart sensor networks [14].

II. Overview on the Measurement System

A. Theoretical Background on MLS-Based Measurements

The architecture of the proposed measurement system is depicted in Fig. 1. The principle makes use of MLS sequences as excitation signal for the analog front-end (AFE). These sequences are generated through linear feedback shift registers (LFSRs), which can be implemented as cost-effective digital circuits or as efficient firmware algorithms. Let $m[n]$ a generic discrete-time MLS signal generated by an Lth order LFSR, thus having $N_M = 2^L - 1$ binary symbols. An interesting feature of the MLS regards the similarity between its periodic autocorrelation function (ACF), $\phi_{mm}[n]$, and the Kronecker delta impulse, $\delta[n]$. The ACF can be derived as follows [13], [15]:

$$\phi_{mm}[n] = \frac{1}{N_M}\sum_{i=0}^{N_M-1} m[i]\cdot m[n+i] = \frac{N_M+1}{N_M}\cdot\delta[n] - \frac{1}{N_M} \tag{1}$$

where the $[n+i]$ index sum is evaluated mod N_M. With reference to Fig. 1, let us consider a linear and time-invariant (LTI) system, $H(s)$, expressed as a continuous-time transfer function in the Laplace domain. This system includes the AFE which is connected to the IDC sensor. An LTI AFE, with a first-order transfer function, is assumed with the following expression in the Laplace domain:

$$H(s) = \frac{H_0}{s\cdot\tau + 1} \tag{2}$$

where H_0 is the dc gain of the system and τ is the time constant. The time-domain IR from (2) is obtained through the inverse Laplace transform as follows:

$$h(t) = \frac{H_0}{\tau}\cdot e^{-\frac{t}{\tau}}. \tag{3}$$

The discrete-continuous time conversion is performed by a zero-order hold (ZOH) block at the input of the LTI system, which generates the continuous-time input signal,

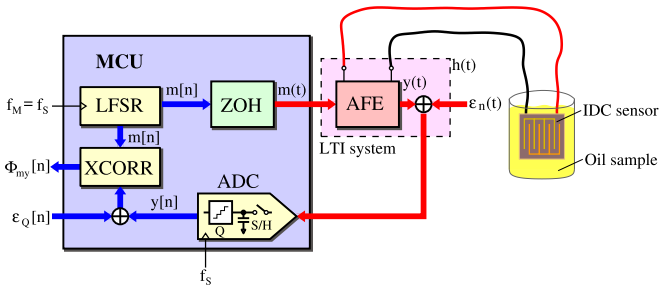

Fig. 1. Architecture of the proposed system.

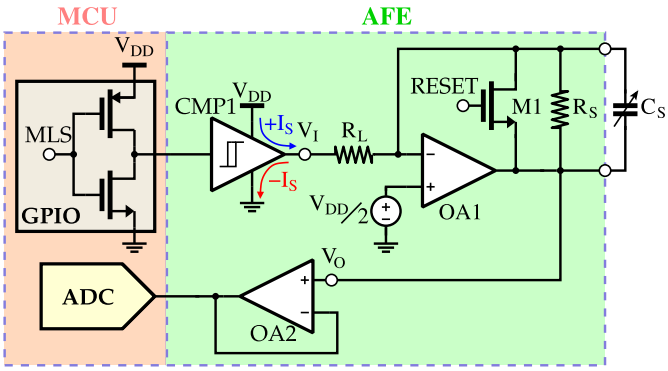

Fig. 2. Circuit schematic of the implemented AFE.

$m(t)$, by holding each binary sample value of $m[n]$ constant over the T_S time interval. The system's output, $y(t)$, is then digitized by the analog-to-digital converter (ADC), giving the $y[n]$ discrete-time sequence. The ADC operates with $f_S = 1/T_S$ sampling frequency and N_R resolution expressed in bits. It is worth noting that the ADC sampling period, T_S, has been selected equal to the ZOH interval.

Regarding the AFE, the architecture in Fig. 2 has been implemented. It acts as a low-pass active filter with the following parameters:

$$H_0 = -\frac{R_S}{R_L} \tag{4}$$

$$\omega_S = \frac{1}{\tau} = \frac{1}{R_S \cdot C_S}. \tag{5}$$

By substituting (4) and (5) in (3), the following AFE's IR is obtained:

$$h(t) = -\frac{1}{R_L \cdot C_S} \cdot e^{-\frac{t}{R_S \cdot C_S}}. \tag{6}$$

The result of 1 is exploited in the circular cross correlation, $\phi_{\text{my}}[n]$, between the MLS input sequence, defined as $m_V[n] = V_S \cdot m[n]$, and the output sequence, $y[n]$, as follows [13], [16], [17]:

$$\begin{aligned}\phi_{\text{my}}[n] &= \frac{1}{N_M} \sum_{i=0}^{N_M-1} m_V[i] \cdot y[n+i] \\ &\approx V_S^2 \cdot T_S \cdot \left(h[n] \cdot u[n-1] - \frac{H_0}{N_M \cdot T_S} \right)\end{aligned} \tag{7}$$

where V_S is the voltage amplitude of the MLS signal, $h[n] \triangleq h(n \cdot T_S)$ is the discrete-time expression of $h(t)$, and $u[n-1]$ is the discrete-time step function. The latter comes from the inverse Zeta transform of the transfer function obtained by multiplying the discrete-time version of (6) by the transfer function of the ZOH, as derived in [13]. Thus, considering a high N_M value, the measured discrete-time IR of the AFE, that is, $h[n]$, can be obtained as follows:

$$\begin{aligned}\frac{\phi_{\text{my}}[n]}{V_S^2 \cdot T_S} &\approx h[n] \cdot u[n-1] \\ &= \begin{cases} -\dfrac{1}{R_L \cdot C_S} \cdot e^{-\frac{n \cdot T_S}{R_S \cdot C_S}}, & 1 \le n \le N_M \\ 0, & n = 0. \end{cases}\end{aligned} \tag{8}$$

It is important to point out that, due to the periodic nature of the circular cross-correlation operation, multiple MLS cycles are generally required to reach the periodic steady state in $\phi_{\text{my}}[n]$. This is essential to obtain an accurate AFE's IR measurement. Regarding the proposed AFE, simulations proved that a first MLS cycle is enough to reach the periodic steady state while the actual $y[n]$ measurement, through ADC, can be performed during a second cycle. Then, considering two MLS cycles for measurements, the requested time interval for the excitation is

$$t_{\text{exc}} = 2 \cdot N_M \cdot T_S. \tag{9}$$

Two main error sources play a role in degrading the accuracy of the measured IR and are the electronic noise of the AFE, ε_n, and the quantization noise of the ADC, ε_Q. These sources are reported in Fig. 1 as additive independent and identically distributed (i.i.d.) random signals and are detailed in [13]. As an example of the MLS-based measurement technique, Fig. 3 shows a simulated IR (blue samples) obtained by implementing the measurement system of Fig. 1 in MATLAB environment. Here, the following parameters have been used for the simulation: R_L equal to 374 kΩ, R_S equal to 100 kΩ, an arbitrary C_S equal to 330 pF, V_S equal to 1.5 V, f_S equal to 125 kHz, N_M equal to 1023, a resolution of 10 bit for the ADC, and an ideal opamp model with both infinite gain and bandwidth.

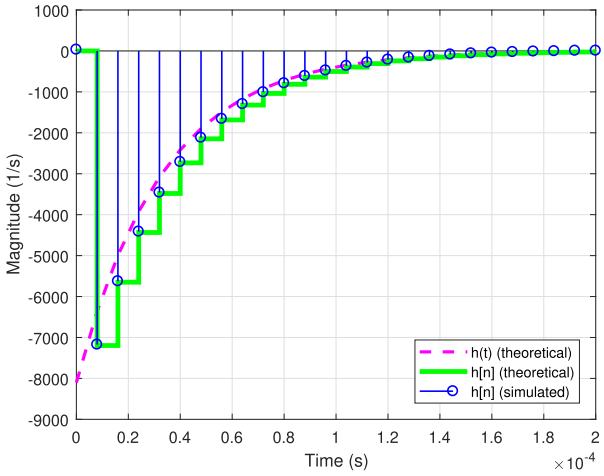

Fig. 3. Theoretical versus simulated IR obtained through MATLAB simulation of the AFE.

B. Proposed Measurement Approach

The measured IR, obtained through the cross correlation in (7), is exploited for the indirect measurement of the moisture concentration in lubricant oil. More specifically, the variation of the dielectric constant through the variation of the sensor's capacitance, C_S, is investigated as the sensor is immersed in oil–water mixtures. The analytical model presented in [18], [19], and [20] for gas-sensitive IDCs is used as a starting point to describe, in first approximation, the behavior of the adopted IDC sensor as the gas is substituted with lubricant oil. By considering the height of the sensitive layer much smaller than the electrodes' width and by neglecting the imaginary part of the complex dielectric permittivity of all materials, the C_S can be approximated with the sum of two contributions

$$C_S \approx \left(\varepsilon_{\text{CO},T} + \varepsilon_s\right) \cdot C_K \tag{10}$$

where $\varepsilon_{\text{CO},T}$ is the relative permittivity of the water-contaminated lubricant oil at T temperature, ε_s is the permittivity of the substrate, and C_K is a proportionality factor which depends on IDC geometry. The temperature plays a role in the change of oil's permittivity. However, as found in [21], the permittivity variation due to the temperature is significantly lower with respect to the variation due to the water content. As detailed in Section III-A, the metal electrodes are separated from the silicon substrate by a

SiO_2 layer which is much thinner than the silicon. According to [22], which reports the general case of composite dielectric, the contribution of the thin SiO_2 layer can be neglected in the equivalent dielectric constant, thus, only the silicon value, equal to 11.7, is considered for ε_s. For theoretical calculations, an approximate value for C_K has been derived from finite-element method (FEM) simulation by considering the sensor's sensitive layer immersed in air and, thus, having $\varepsilon_{CO,T}$ equal to 1. Once the sensor's capacitance in air, $C_{S,\text{air}}$ is obtained from the simulated IDC, C_K is derived from (10) as follows:

$$C_K = \frac{C_{S,\text{air}}}{1+\varepsilon_s} \approx 25 \text{ pF}. \tag{11}$$

The $C_{S,\text{air}}$ value from FEM, equal to 320 pF, was chosen in (11) since the ε_s used in FEM is also considered. For water concentrations, φ_W, under 3 vol%, the following approximated expression for $\varepsilon_{CO,T}$ can be considered [21]:

$$\varepsilon_{CO,T} \approx \varepsilon_{O,T} \cdot (1 + 3 \cdot \varphi_W) \tag{12}$$

where $\varepsilon_{O,T}$ is the permittivity of the pure oil at T temperature, ranging from 2.1 to 2.8 for lubricant oils [23]. The volume percent concentration, vol%, is hereinafter expressed with the % symbol. By substituting (12) in (10), the following approximate relationship between C_S and φ_W is obtained:

$$C_S \approx \left[\varepsilon_{O,T} \cdot (1 + 3 \cdot \varphi_W) + \varepsilon_s\right] \cdot C_K. \tag{13}$$

By assuming an ideal first-order behavior of the AFE, while connected to the IDC sensor, the C_S value can be obtained through the measure of $h[n] \cdot u[n-1]$. However, instead of a full cross-correlation calculation over all N_M samples, the proposed measurement approach aims to compute a single cross-correlation point to speed up the overall measurement time. The choice of the n index for the single measurement is made to maximize the relative sensitivity of $h[n]$ with respect to C_S. The following expression for the relative sensitivity is obtained:

$$S_{C_S}^{h_n} = \frac{\partial h[n]}{\partial C_S} \cdot \frac{C_S}{h[n]} = \left| \frac{n \cdot T_S}{R_S \cdot C_S} - 1 \right|. \tag{14}$$

Equation (14) is maximized by n equal to 1, that is, the second sample, being n an integer greater or equal to 1. However, as explained in Section IV, the choice of the second sample results is unrealistic from a practical point of view. More specifically, preliminary tests showed that the system exhibits the assumed first-order behavior, that is, the typical exponential function, starting from the third sample. Thus, the $h[2]$ sample is chosen. From (8), the following expression can be derived:

$$h_{pk} = h[2] = -\frac{\psi_2}{R_L \cdot C_K \cdot \left(\varepsilon_s + \varepsilon_{O,T} + 3 \cdot \varepsilon_{O,T} \cdot \varphi_W\right)} \tag{15}$$

where the R_L resistor is a design parameter of the AFE and ψ_1 is the following exponential term which, by assuming $T_S \ll R_L \cdot C_K$ and a small φ_W value, can be approximated as follows:

$$\begin{aligned} \psi_2 &= e^{-\frac{2 \cdot T_S}{R_L \cdot C_K \cdot \left(\varepsilon_s + \varepsilon_{O,T} + 3 \cdot \varepsilon_{O,T} \cdot \varphi_W\right)}} \\ &\approx 1 - \frac{2 \cdot T_S}{R_L \cdot C_K \cdot \left(\varepsilon_s + \varepsilon_{O,T}\right)}. \end{aligned} \tag{16}$$

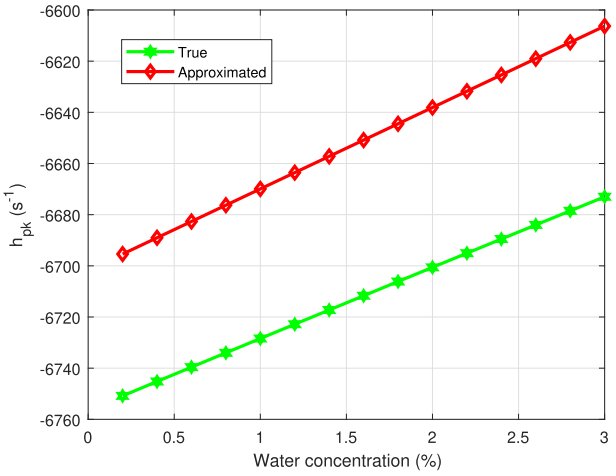

Fig. 4. Graphical representations of true and linearized expressions of h_{pk}.

Keeping the assumption of small φ_W, (15) can be linearized through Taylor series expansion at first order, giving the following relationship:

$$h_{pk} \approx -\frac{\psi_2}{R_L \cdot C_K \cdot \left(\varepsilon_s + \varepsilon_{O,T}\right)} \cdot \left(1 - \frac{3 \cdot \varepsilon_{O,T}}{\varepsilon_s + \varepsilon_{O,T}} \cdot \varphi_W\right). \tag{17}$$

Equation (17) shows, in first-order approximation, the relationship between low moisture contamination in lubricant oil, φ_W, and the measurement of the IR's peak, h_{pk}. The linearity of (17) is verified in Section IV-B through experimental measurements, with concentrations in the $0.2\% \div 3\%$ range. The acceptable contamination values of water in oil greatly depend on the application. For instance, a 3% concentration is still tolerable for the wind turbine application [21], whereas the stricter value of 0.2% is the maximum tolerable concentration in the automotive field [24]. Regarding the validity of h_{pk} approximation, for φ_W under 3%, it is verified by plotting both (15) and (17) with an R_L of 374 kΩ, a C_K of 25 pF, a ε_s of 11.7, and a $\varepsilon_{O,T}$ of 2.2. The curves are depicted in Fig. 4, exhibiting a maximum error, between true and approximated h_{pk}, of 1%.

As already mentioned, the derivation of the h_{pk} value, instead of a full $h[n]$ measurement, is advantageous since, according to (7), it takes only N_M multiply-accumulate (MAC) operations, compared to N_M^2 MACs of a full IR. The time needed to perform such calculation is added to (9) to obtain the total time which is required for an h_{pk} measurement. This time results, from experimental measurements, to be close to 18 ms.

C. AFE Design

The circuit schematic of the implemented AFE is depicted in Fig. 2. The MLS sequence is provided by a general purpose input–output (GPIO) peripheral of the microcontroller unit (MCU), which is configured as a digital output. This GPIO also performs the ZOH operation. The MLS signal is then buffered by the Schmitt trigger buffer CMP1 (SN74LVC1G17, Texas Instruments) and, thus, fed in the analog circuit

composed by OA1 and OA2 opamps, the M1 MOSFET, the R_L resistor, the R_S feedback resistor, and the C_S capacitive sensor. The MCP6022 opamp was chosen for the application. Given the V_{DD} supply voltage of the circuit, the voltage reference $V_{DD}/2$ is generated through a precision voltage reference (REF2030, Texas Instruments). This voltage reference is connected to the positive terminal of the OA1 opamp. By choosing this reference, the voltage amplitude for the MLS, V_S, becomes equal to $V_{DD}/2$.

The analysis presented in Section II-B is further expanded here to derive the design equations for the AFE. With reference to (17), the absolute sensitivity of the h_{pk} parameter, with respect of the φ_W water concentration, is derived as follows:

$$S = \frac{\partial h_{pk}}{\partial \varphi_W} \approx \frac{\Delta h_{pk}}{\Delta \varphi_W} = \frac{3 \cdot \psi_2}{R_L \cdot C_K} \cdot \frac{\varepsilon_{O,T}}{\left(\varepsilon_s + \varepsilon_{O,T}\right)^2}. \tag{18}$$

From (18), the minimum h_{pk} variation, $\Delta h_{pk,\min}$, is derived in response to a minimum φ_W variation, $\Delta\varphi_{W,\min}$

$$\Delta h_{pk,\min} = \frac{3 \cdot \psi_2}{R_L \cdot C_K} \cdot \frac{\varepsilon_{O,T}}{\left(\varepsilon_s + \varepsilon_{O,T}\right)^2} \cdot \Delta\varphi_{W,\min} \tag{19}$$

$\Delta h_{pk,\min}$ and $1/\Delta h_{pk,\min}$ are considered the range and the height, respectively, of a statistical uniform distribution which describes the variation of h_{pk} in response to a minimum variation of water. The standard deviation of this distribution can be written as follows:

$$\sigma_m = \frac{\Delta h_{pk,\min}}{\sqrt{12}}. \tag{20}$$

To correctly measure the minimum variation of h_{pk} in response to the minimum variation of φ_W, the standard deviation in (20) must be greater than the standard deviation of the measurement error which has been characterized in [13]. In mathematical terms, the following condition must be met:

$$\sigma_m > \sigma_h = \frac{\sqrt{\sigma_Q^2 + \sigma_n^2}}{\sqrt{N_M} \cdot V_S \cdot T_S} \tag{21}$$

where σ_Q and σ_n are the standard deviations of the quantization noise, due to the analog-to-digital conversion, and the noise of the AFE, respectively. σ_Q has the following expression:

$$\sigma_Q = \frac{V_{FS}}{\sqrt{12} \cdot \left(2^{N_R} - 1\right)} \tag{22}$$

where V_{FS} if the full-scale voltage, equal to 3 V, and N_R is the resolution, in terms of an effective number of bits, of the ADC. Regarding the σ_n term, it has been derived for the proposed AFE in [13]. By considering only the thermal noise contribution in the circuit and neglecting the opamp's noise contributions, the following expression of integrated output noise can be used:

$$\sigma_n \approx \sqrt{\frac{k \cdot T}{C_S} \cdot \left(1 + \frac{R_S}{R_L}\right)} \tag{23}$$

where k is the Boltzmann constant and T is the temperature in K. From (23), it can be seen that for high R_L, the σ_n tends to its minimum which is $(k \cdot T/C_S)^{1/2}$ which, in turns, can be neglected with respect of σ_Q. Thus, (21) condition is simplified as follows:

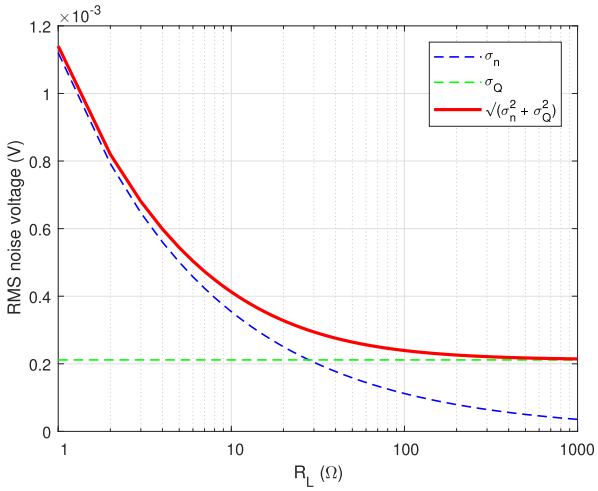

Fig. 5. Graphical representations of standard deviations of noise sources in the AFE versus the R_L value.

$$\sigma_m > \frac{\sigma_Q}{\sqrt{N_M} \cdot V_S \cdot T_S}. \tag{24}$$

By substituting (19) in (20), and by substituting the result in (24), the following upper bound for R_L is obtained:

$$R_L < \frac{3}{2} \cdot \frac{\psi_2 \cdot \Delta\varphi_{W,\min}}{C_K} \cdot \frac{\varepsilon_{O,T}}{\left(\varepsilon_s + \varepsilon_{O,T}\right)^2} \cdot \sqrt{N_M} \cdot T_S \cdot \left(2^{N_R} - 1\right). \tag{25}$$

By using a $\varphi_{W,\min}$ of 0.2 %, a C_K of 25 pF, an N_M of 1023, a T_S of 8 µs, an N_R of 12 bits, a ε_s of 11.7, and an $\varepsilon_{O,T}$ of 2.2, and an upper bound of about 1.2 MΩ is obtained for R_L. The assumption by which σ_n can be neglected with respect to σ_Q is valid for high values of R_L. By decreasing the R_L value, σ_n increases until it becomes comparable with σ_Q. As an example, Fig. 5 shows the standard deviations of noise sources versus the R_L value. The following parameters have been considered for the plot: V_{FS} equal to $2 \cdot V_S = 3$ V, N_R of 12 bits, T equal to 300 K, $C_S = C_{S,\min}$ of 330 pF, and an R_S of 100 kΩ. The $C_{S,\min}$ value of 330 pF is approximately the experimental value of the sensor in pure oil. The figure shows that to optimize the noise performance of the AFE, a relatively high R_L must be ensured to keep the constant σ_Q term dominant with respect to σ_n. More specifically, by solving the condition by which σ_Q must be greater than σ_n, the following lower bound for R_L is obtained:

$$R_L > \frac{R_S}{\frac{\sigma_Q^2}{kT/C_{S,\min}} - 1}. \tag{26}$$

The $C_{S,\min}$ value is used in (26) since it gives the highest noise value and, thus, the higher lower bound for R_L. By substituting the aforementioned parameters in (26), a resistance value of 28 Ω is obtained as lower bound for R_L.

Regarding the selection of R_S value, its lower bound can be determined through a consideration of the maximum working frequency of the system. According to [9], the f_S MLS frequency must be greater than 3× the maximum system's

frequency, that is, the AFE's pole which is equal to $1/(2\pi \cdot \tau)$. This rule of thumb comes from the frequency response of the ZOH block which shapes the ideally flat spectrum of the MLS as a sinc-shaped low-pass filter with a cut-off frequency of $f_S/3$. The maximum usable f_S depends on the adopted microcontroller's timing and on the firmware implementation of the system. In particular, high f_S values give place to synchronization issues between the timer peripheral, which generates the timing for the MLS, and the synchronous acquisition of the ADC. To measure an accurate IR from the cross-correlation operation, the synchronization between input and output signals ($m[n]$ and $y[n]$ in Fig. 1) must be ensured. It turns out from practical tests that the maximum selectable $f_S = f_{S,\text{MAX}}$ value is 125 kHz. This value guarantees the highest MLS frequency with the best synchronization performance. Thus, by imposing the AFE's pole, $1/(2\pi \cdot \tau)$, smaller than $f_S/3$, the following lower bound of R_S is obtained:

$$R_S > \frac{3}{2\pi \cdot C_{S,\text{min}} \cdot f_{S,\text{MAX}}}. \tag{27}$$

Similar to (26), the $C_{S,\text{min}}$ value is used in (27) since it gives the maximum supported AFE's pole. A lower bound equal to 3.8 kΩ is obtained for R_S. An upper bound for R_S can be derived by taking into account the saturation of the OA1 opamp. Since a rail-to-rail opamp was adopted, the following condition is considered:

$$\left| V_O - \frac{V_{DD}}{2} \right| = \left| -m[n] \cdot \frac{R_S}{R_L} \cdot \frac{V_{DD}}{2} \right| \leq \frac{V_{DD}}{2} \tag{28}$$

which leads to

$$R_S \leq R_L. \tag{29}$$

To optimize the tradeoffs in terms of the system's noise, bandwidth, accuracy, and output range, the values of 374 and 100 kΩ have been selected for R_L and R_S, respectively.

III. Implementation Details

A. Sensor Design and Fabrication

The sensor comprises a pair of interdigitated electrodes, each including 46 fingers with a width and gap size of 20 µm and length of 6560 µm. It has an active area of 24.3 mm^2 and it was realized on a 4″ (100) Si/SiO_2 wafer (500 nm thermal oxide) by using 365 nm UV optical lithography, RF sputtering deposition of 20 nm-thick titanium adhesion layer and 200 nm-thick gold layer, and lift-off process. FEM simulations using COMSOL multiphysics were used to design the sensor by optimizing its sensitivity versus different values of oil's relative permittivity within the range of interest for the application. Fig. 6 depicts a cross-sectional view of the sensor, comprising two adjacent metal fingers separated from the silicon substrate by a 500 nm thick SiO_2 layer. The electric field lines penetrate the liquid as well as the substrate layer, and the electric field distribution changes with $\varepsilon_{\text{CO},T}$ affecting the sensor capacitance. The relative sensitivity of the sensor's capacitance in response to changes in dielectric constant is studied, through simulation, to identify the finger width and gap size which optimize the sensitivity. Fig. 7 shows its variation for increasing values of width finger and gap size in the range 20–80 µm and for increasing values of $\varepsilon_{\text{CO},T}$. As the sensitivity improves with smaller electrode width and gap size, the optimal value of these parameters was set to 20 µm, obtaining the best compromise between sensing performance and technological reliability of the device.

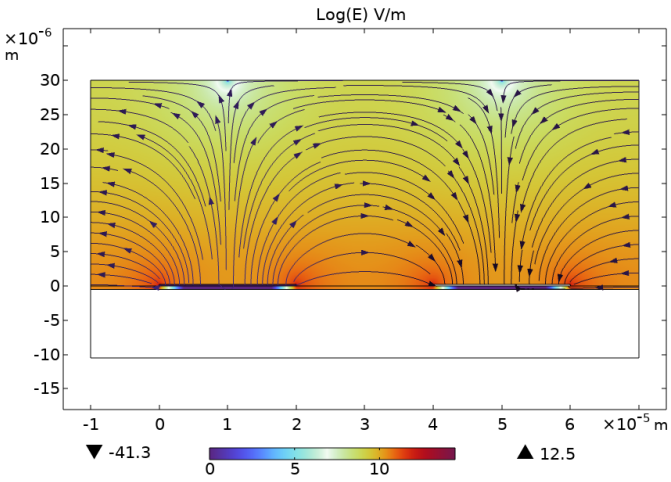

Fig. 6. Electric field distribution (log scale) between two adjacent electrodes. The field lines penetrate the dielectric medium ($\varepsilon_{\text{CO},T} = 2.2$) and the insulation layer underneath the electrodes.

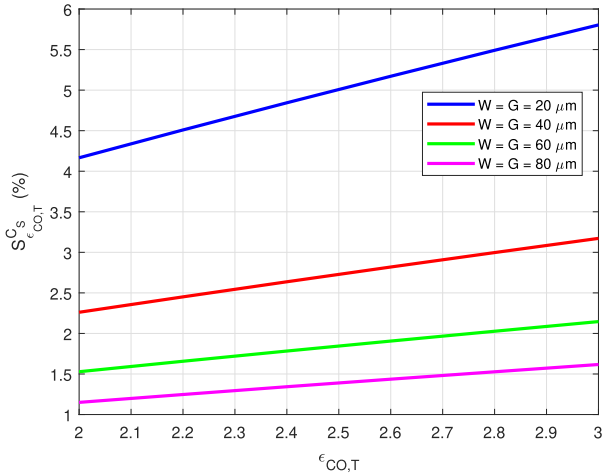

Fig. 7. Sensitivity variation for increasing values of $\varepsilon_{\text{CO},T}$, at varying values of width finger, W, and gap size, G, in the range 20–80 µm.

B. Description of the Electronic System

A block diagram of the measurement board and a photograph of the interfacing system are depicted in Figs. 8 and 9, respectively. The *MultiSense V2* mainboard (white board in Fig. 9) has been adopted. It is a general-purpose multichannel acquisition and actuation platform for research-related applications. The AFE expansion module (green board in Fig. 9) implements the circuit schematic of Fig. 2. The functional modules are: 1) power management controller (PMC); 2) communication peripherals; 3) AFE circuit; 4) pneumatic actuation module (PWR ACT and pump controller); 5) led and switches; and 6) the MCU section. The board/user interaction is managed through the micro-USB

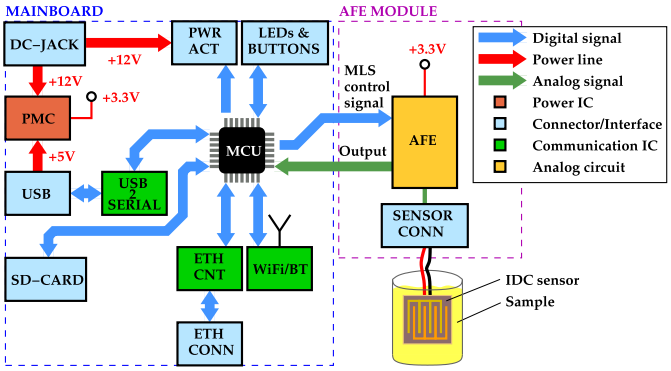

Fig. 8. Simplified architecture of the measurement system.

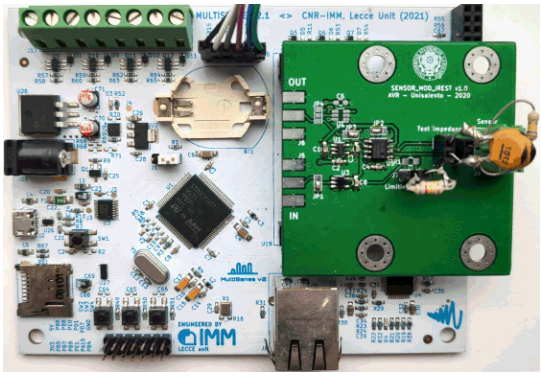

Fig. 9. Photograph of the realized measurement system (motherboard + AFE).

connector which provides both the 5 V supply voltage and the serial-over-USB communication. The system operations, including the generation of excitation signal for the IDC sensor and the measurements, are carried out by the STM32F407 (ST Microelectronics) microcontroller whose clock frequency is 100 MHz. Measurement data are sent from the board to the PC through serial-over-USB communication and are processed with MATLAB environment. As the board parses the *START* command from the user, the M1 MOSFET in Fig. 2 is activated through a digital pin. This resets the residual charge of the C_S sensor. The signal acquisition from the ADC was obtained through the direct memory access (DMA) peripheral of the MCU.

IV. Experimental Section

A. Samples Preparation and Preliminary Measurements

The validity of the proposed approach was verified through experimental measurements. More specifically, the assessment of moisture contamination, ranging from 0.2% to 3%, was investigated in commercial fresh lubricant oil for aviation, that is, the AeroShell Turbine Oil 500, produced by Shell. Five water–oil samples were prepared with nominal water concentrations of 0.2%, 0.5%, 1%, 2%, and 3%. To produce accurate concentrations, an analytical balance (ABT 120-5DNM, manufactured by KERN and SOHN GmbH) was used. The weight is thus considered, instead of the volume, for the preparation of samples. This implies an error in the final volumetric concentrations due to the different densities of oil and water. In particular, the following

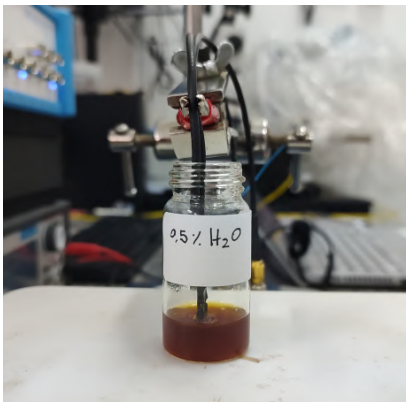

Fig. 10. Photograph of a water–oil sample under measurement.

equation is used to relate the mass percent, $C_{\text{wt\%}}$, to the volume percent, $C_{\text{vol\%}}$:

$$C_{\text{vol\%}} = \frac{m_{\text{H}_2\text{O}} \cdot \rho_{\text{oil}}}{m_{\text{oil}} \cdot \rho_{\text{H}_2\text{O}} + m_{\text{H}_2\text{O}} \cdot \rho_{\text{oil}}} \cdot 100 = \frac{1}{1 + \frac{\rho_{\text{H}_2\text{O}}}{\rho_{\text{oil}}} \cdot \frac{100 - C_{\text{wt\%}}}{C_{\text{wt\%}}}} \cdot 100 \tag{30}$$

where m_{oil} is the mass of oil which was fixed equal to 5 g for all samples, $m_{\text{H}_2\text{O}}$ is the mass of the water, ρ_{oil} is the density of the oil which is specified by the manufacturer equal to 1005 kg/m^3 at 15 °C, and $\rho_{\text{H}_2\text{O}}$ is the density of water equal to 999.1 kg/m^3 at 15 °C. As a result, the true $C_{\text{vol\%}}$ concentrations are: 0.2012 vol%, 0.5029 vol%, 1.0058 vol%, 2.0116 vol%, and 3.0172 vol%. The u_C uncertainty in the $C_{\text{vol\%}}$, due to the weighing process, can be analyzed by considering δ_m as the balance's uncertainty, m_{oil} and $m_{\text{H}_2\text{O}}$ as uncertainty variables, and by using the uncertainty propagation formula on (30). The following equation can be derived:

$$u_c = k \cdot \delta_m \frac{\rho_{\text{H}_2\text{O}} \cdot \rho_{\text{oil}} \cdot \sqrt{m_{\text{oil}}^2 + m_{\text{H}_2\text{O}}^2}}{\left(m_{\text{oil}} \cdot \rho_{\text{H}_2\text{O}} + m_{\text{H}_2\text{O}} \cdot \rho_{\text{oil}}\right)^2} \cdot 100 \tag{31}$$

where k is the coverage factor of the expanded uncertainty. According to [25], δ_m is obtained by combining the balance's uncertainties due to readability, repeatability, and linearity which are specified in [26]. They are equal to 0.1, 0.1, and 0.2 mg, respectively. By assuming a rectangular distribution for these uncertainties, a δ_m of 0.14 mg is derived. From (31), the expanded uncertainties for the five prepared concentrations are equal to ±0.0057 vol%, ±0.0056 vol%, ±0.0056 vol%, ±0.0055 vol%, and ±0.0054 vol%, respectively. These are specified with a k coverage factor of two which gives a level of confidence of approximately 95%. Prepared samples were treated by sonication procedure (using the Sonicator 700 W, manufactured by Fisher Scientific), to obtain stable emulsions with extremely small internal droplets. A photograph of a prepared sample is depicted in Fig. 10. The measurements were performed at room temperature, that is, 300 K, by immersing the IDC sensor in the prepared samples. The entire IR was obtained for all the prepared samples and the results are depicted in Fig. 11. The required measurement time for a complete IR (1023 points) is 700 ms. The figure shows that the measured IR points for pure oil sample well

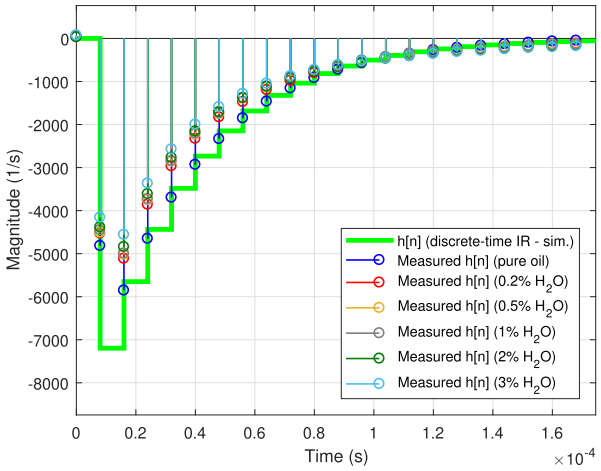

Fig. 11. Preliminary IR measurements of the IDC sensor in water–oil samples.

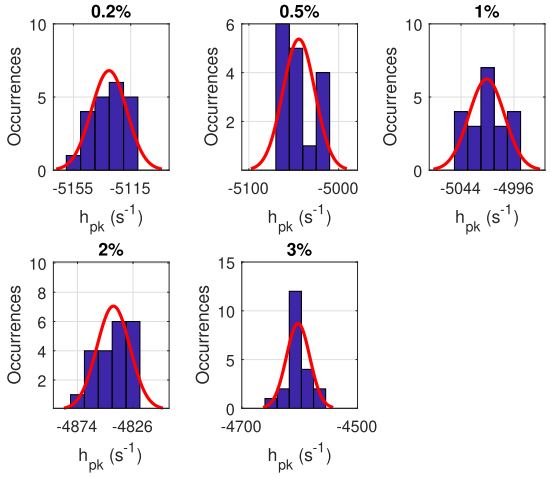

Fig. 12. Histograms of h_{pk} measurements.

overlay over the theoretical IR obtained by considering a C_S of 330 pF. This capacitance value has been estimated through IS with conventional laboratory instrumentation. With the increase of the water concentration, the IR amplitude decreases as expected. However, this preliminary test also shows evidence concerning the difference between theoretical and real models of the measurement system. It can be noted by graphical inspection of Fig. 11 that, differently from the ideal case, the typical first-order behavior, that is the exponential function, starts from n equal to 2, that is, the third sample. This is because the real measurement system, composed of AFE, IDC sensor, liquid sample, electrical connections, connectors, parasitic capacitors, and so on, is not a perfect first-order system as it has been assumed in (2), but it exhibits a more complex frequency behavior. Thus, the h_2 sample is selected as the maximum-sensitivity point and as h_{pk}.

B. Experimental Results

The following parameters have been used for the hardware implementation of the AFE: R_L equal to 374 kΩ, R_S equal to 100 kΩ, V_S equal to 1.5 V, f_S equal to 125 kHz, N_M equal to 1023, and an ADC resolution of 12 bits. Twenty

TABLE I
STATISTICAL CHARACTERIZATIONS OF h_{pk} MEASUREMENTS

φ_w	μ (s^{-1})	σ (s^{-1})
0.2%	-5130.13	12.3129
0.5%	-5044.32	17.8075
1%	-5020.72	16.1378
2%	-4842.93	14.2522
3%	-4602.75	20.2272

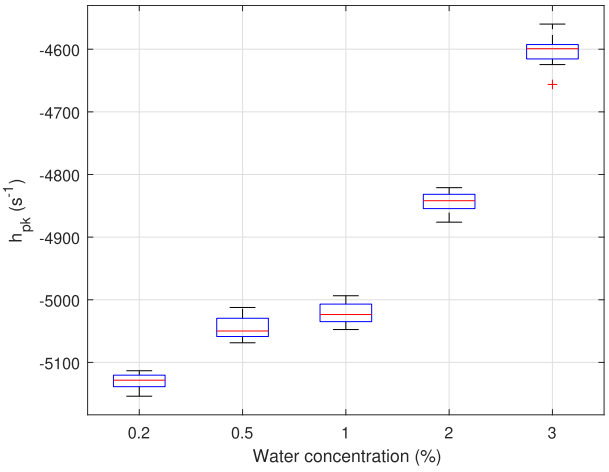

Fig. 13. Box plot of the measured h_{pk} samples.

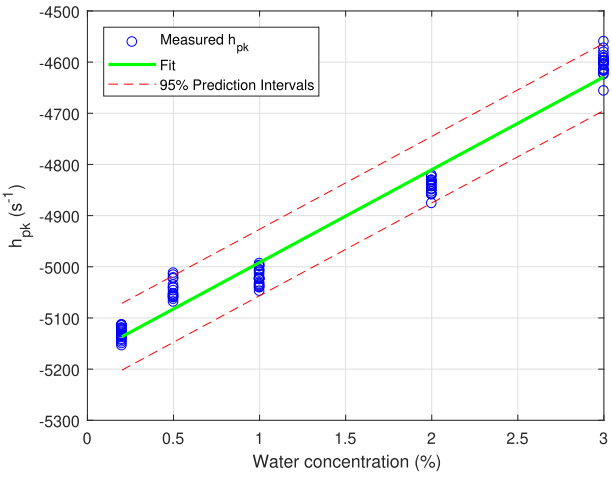

Fig. 14. Linear fitting of the measured h_{pk} samples.

repeated measurements of the h_{pk} parameter were carried out for the prepared samples and they are depicted in Fig. 12. A Gaussian fitting was carried out for every concentration and the results, in terms of mean and standard deviation, are reported in Table I.

Measured data are represented, for each nominal water concentration, in the box plot of Fig. 13. The central red mark in the boxes indicates the median, while the top and bottom edges indicate the 25th and 75th percentiles, respectively. A single outlier is identified with the red cross at the 3% concentration. Fig. 14 shows a linear fitting of the measured h_{pk} samples along with the 95% prediction interval, that is, about the $\pm 2\sigma$ interval assuming a normal distribution of the measurements. The σ calculated from the residuals

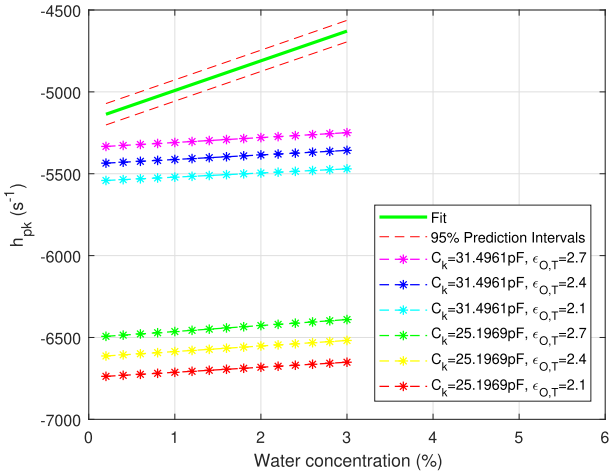

Fig. 15. Comparison between theoretical model and linear fitting of the measured h_{pk} samples.

is 32.4 s^{-1}. A very good R^2 of 0.97 was obtained from the fitting, confirming the validity of the linear approximation to explain the relationship between the measured parameter, that is, h_{pk}, and low moisture concentration. A slope, that is the absolute sensitivity of the linear model, of 181.3 $s^{-1}/\%$ is obtained. The fitted model was compared with the theoretical model in (17) and the results are depicted in Fig. 15. In particular, (17) is plotted by varying C_K and $\varepsilon_{O,T}$ parameters which change with the sensor's geometry and oil conditions in terms of temperature, aging, and other contaminants. Both the difference in offset and slope, between theoretical and fitted experimental curves, are imputable to the approximations made during the derivations, such as the assumption of constant temperature of the samples, linear relationship between dielectric constant and water concentration, and so on. This strong variability in offset and slope also suggests that a one-time calibration procedure must be performed before system operation. However, the developed model supports the validity of the proposed linearized approach for the measurement of small water concentration in lubricant oil.

The LOD parameter was derived, for the proposed system, by using the equation in [6]

$$\mathrm{LOD} = \left| \frac{3 \cdot \sigma_b \cdot \varphi_{W,\min}}{\overline{h_{pk,\min}}} \right| \tag{32}$$

where σ_b is the standard deviation of the blank measure, intended as the measure in pure oil, and $\overline{h_{pk,\min}}$ is the average value of $h_{pk,\min}$. The ppm value from (32) is obtained by multiplying the result by 10^6. An LOD of 6.3 ppm is obtained with a σ_b of 5.4 s^{-1}, a $\varphi_{W,\min}$ of 0.002 vol/vol, and a $\overline{h_{pk,\min}}$ of -5130 s^{-1}. As stated in Section II-B, the obtained measured time for h_{pk} is close to 18 ms. This time comes from the sum between the excitation time and the digital-signal-processing time as follows:

$$t_{\mathrm{meas}} = t_{\mathrm{exc}} + t_{\mathrm{DSP}} = \alpha \cdot T_{\mathrm{CLK}} \tag{33}$$

t_{exc} is derived from (9) by taking into account the T_S period time which is obtained by multiplying the clock period, T_{CLK}, by 800. t_{DSP} is directly measured on the STM32F407 MCU through the CYCCNT register. This is a free-running register, provided by the ARM architecture, which is incremented on each cycle of the 100 MHz processor clock. A CYCCNT value of 160 531 is derived during the processing. Thus, the α factor in (33) is equal to 1 797 331, giving an exact value for t_{meas} of 17.97 ms. The uncertainty of this can be evaluated by considering the jitter of the MCU's PLL, which is responsible for the generation of the 100 MHz clock signal. This jitter is specified in [27] as rms period jitter which is defined as the standard deviation of the clock period measurements over a large number of cycles. In this calculation, a Gaussian distribution for the jitter is assumed. More specifically, it turns out that the u_t uncertainty of the t_{meas} is

$$u_t = k \cdot \alpha \cdot \delta T_{\mathrm{CLK}} \tag{34}$$

where k is the coverage factor of the expanded uncertainty and δT_{CLK} is the rms period jitter which has been specified equal to 15 ps for the internal PLL of the used MCU. By substituting the values, the following measurement time can be declared:

$$t_{\mathrm{meas}} = (17.97 \pm 0.054)\ \mathrm{ms}. \tag{35}$$

The reported expanded uncertainty is calculated using a coverage factor, k, of two which gives a level of confidence of approximately 95%.

Table II shows a state-of-the-art comparison of sensing systems for moisture contamination assessment. The standout feature is the measurement time, which is much lower when compared with other solutions. Moreover, differently from [4] and [6], the proposed system adopts a miniaturized embedded system for both measurement, including both the AFE and the signal processing. This permits us to realize a smaller and lighter system with a much lower power consumption

TABLE II
STATE-OF-THE-ART OF MOISTURE CONTAMINATION ASSESSMENT SYSTEMS

	[6]	[4]	[5]	**This work**
Sensing principle	Electrical resonator	Ultrasonic	Permittivity change	**Permittivity change + MLS**
Meas. approach	Impedance	Wave propag. meas.	Impedance	**IR meas.**
Meas. system	Lab. instr. (network analyzer)	Lab. instr.	Custom mainboard + commercial AFE (AD5933)	**Custom Mainboard + AFE**
Min. tested water conc.	0.0025%	0.1%	0.05%	**0.2%**
LOD	1 ppm	N/A	N/A	**6.3 ppm**
Linearity (R^2)	N/A	0.98 (max)	0.98	**0.97**
Meas. time	10 min	6 hours for a sample set	N/A	**18 ms**

of 167 mW. This power consumption can be considered as the sum of two separated contributions: 1) the idle power, equal to 166.9 mW, which is the power of the system with all the peripherals (core, ADC, AFE) in on-state and outside the measurement operation and 2) the measurement power, equal to 98 μW, which is the average contribution during a measurement cycle. A similar solution of the adopted sensing technology, with a custom mainboard, has been adopted in [5]. However, the authors use a commercial integrated circuit, that is, the AD5933, which implements the conventional IS which is slower in terms of measurement time. The proposed approach of time-domain impedance, along with the approximated linear model, permits us to take advantage of a faster measurement technique which is also low in terms of computational demand. A single h_{pk} measurement is enough to predict the water concentration in oil. The need for multifrequency excitation and impedance-to-model fitting algorithms, typical of IS systems, is avoided. These advantages make the system suitable for adoption in in-line and battery-powered applications for real-time monitoring of moisture in lubricant oil.

V. Conclusion

In this article, a system and a measurement approach to reduce the measurement time in the assessment of moisture contamination in lubricant oils have been presented. The system is suitable for in-line monitoring and its sensing principle leverages on permittivity change of a custom-made IDC while immersed in lubricant oil. The time-domain impedance concept, that is, the IR, has been exploited here by using MLS binary sequences. Different from conventional IS, MLS-based measurements are performed with simpler hardware, higher computational efficiency, lower power consumption, and lower measurement time. As a novelty, a linear model to relate a single measured quantity from IR to water concentration in oil has been introduced and verified through experimental measurements. This permits to achieve a low measurement time, thus achieving a lower energy-per-measurement parameter. This is a key feature to adopt the proposed measurement approach in battery-powered in-line monitoring devices and smart sensor networks. The validity of the linear model, for the detection of small concentrations of water in lubricant oil, has been verified through experimental measurements. The test has been performed in water–oil prepared samples with 0.2%, 0.5%, 1%, 2%, and 3% concentrations at room temperature, obtaining an estimated LOD of 6.3 ppm. A low measurement time of 18 ms has been achieved, which outperforms with respect to the state-of-the-art.

References

[1] S. Raţiu, A. Josan, V. Alexa, V. G. Cioată, and I. Kiss, "Impact of contaminants on engine oil: A review," *J. Phys., Conf. Ser.*, vol. 1781, no. 1, Feb. 2021, Art. no. 012051.

[2] N. K. Myshkin and L. V. Markova, "Methods and instruments for condition monitoring of lubricants," in *On-line Condition Monitoring in Industrial Lubrication and Tribology* (Applied Condition Monitoring). Berlin, Germany: Springer, Jul. 2017, pp. 1–29.

[3] A. Wolak, "Changes in lubricant properties of used synthetic oils based on the total acid number," *Meas. Control*, vol. 51, nos. 3–4, pp. 65–72, Apr. 2018.

[4] E. Juliastuti, E. W. Tanogono, and D. Kurniadi, "Detection of water content in lubricating oil using ultrasonics," in *Proc. 5th Int. Conf. Instrum., Control, Autom. (ICA)*, Aug. 2017, pp. 188–192.

[5] H. Liu, X. Tang, H. Lu, W. Xie, Y. Hu, and Q. Xue, "An interdigitated impedance microsensor for detection of moisture content in engine oil," *Nanotechnol. Precis. Eng.*, vol. 3, no. 2, pp. 75–80, Jun. 2020.

[6] R. A. Potyrailo et al., "Multivariable electrical resonant sensors for independent quantitation of aging and external contaminants in lubricating oils," *IEEE Sensors J.*, vol. 19, no. 4, pp. 1542–1553, Feb. 2019.

[7] M. Hossain, A. Abu-Siada, and S. Muyeen, "Methods for advanced wind turbine condition monitoring and early diagnosis: A literature review," *Energies*, vol. 11, no. 5, p. 1309, May 2018.

[8] A. V. Radogna, S. Capone, L. Francioso, P. A. Siciliano, and S. D'Amico, "A 177 ppm RMS error-integrated interface for time-based impedance spectroscopy of sensors," *Electronics*, vol. 11, no. 22, p. 3807, Nov. 2022.

[9] G. Luciani, M. Crescentini, A. Romani, M. Chiani, L. Benini, and M. Tartagni, "Energy-efficient PRBS impedance spectroscopy on a digital versatile platform," *IEEE Trans. Instrum. Meas.*, vol. 70, pp. 1–12, 2021.

[10] B. Sanchez, G. Vandersteen, R. Bragos, and J. Schoukens, "Basics of broadband impedance spectroscopy measurements using periodic excitations," *Meas. Sci. Technol.*, vol. 23, no. 10, Aug. 2012, Art. no. 105501.

[11] A. Waligo and P. Barendse, "A comparison of the different broadband impedance measurement techniques for lithium-ion batteries," in *Proc. IEEE Energy Convers. Congr. Expo. (ECCE)*, Sep. 2016, pp. 1–7.

[12] Y. Yang, W. Zhang, F. Du, X. Tang, H. Wen, and Z. Teng, "Broadband bioimpedance spectroscopy based on a multifrequency mixed excitation and Nuttall windowed FFT algorithm," *Math. Problems Eng.*, vol. 2014, pp. 1–9, Jun. 2014.

[13] A. V. Radogna, S. Capone, L. Francioso, P. A. Siciliano, and S. D'Amico, "Performance analysis of an MLS-based interface for impulse response estimation of resistive and capacitive sensors," *IEEE Trans. Circuits Syst. I, Reg. Papers*, vol. 69, no. 9, pp. 3666–3678, Sep. 2022.

[14] F. Corno, L. De Russis, and T. Montanaro, "Estimate user meaningful places through low-energy mobile sensing," in *Proc. IEEE Int. Conf. Syst., Man, Cybern. (SMC)*, Oct. 2016, pp. 3039–3044.

[15] A. V. Radogna, S. D'Amico, S. Capone, and L. Francioso, "A simulation study of an optimized impedance spectroscopy approach for gas sensors," in *Proc. IEEE 8th Int. Workshop Adv. Sensors Interfaces (IWASI)*, Jun. 2019, pp. 142–147.

[16] J. Vanderkooy, "Aspects of MLS measuring systems," *J. Audio Eng. Soc.*, vol. 42, no. 4, pp. 219–231, 1994.

[17] D. D. Rife and J. Vanderkooy, "Transfer-function measurement with maximum-length sequences," *J. Audio Eng. Soc.*, vol. 37, no. 6, pp. 419–444, 1989.

[18] H.-E. Endres and S. Drost, "Optimization of the geometry of gas-sensitive interdigital capacitors," *Sens. Actuators B, Chem.*, vol. 4, nos. 1–2, pp. 95–98, May 1991.

[19] R. H. Bhuiyan, R. A. Dougal, and M. Ali, "Proximity coupled interdigitated sensors to detect insulation damage in power system cables," *IEEE Sensors J.*, vol. 7, no. 12, pp. 1589–1596, Dec. 2007.

[20] A. V. Mamishev, K. Sundara-Rajan, F. Yang, Y. Du, and M. Zahn, "Interdigital sensors and transducers," *Proc. IEEE*, vol. 92, no. 5, pp. 808–845, May 2004.

[21] Y. Du, T. Wu, and R. Gong, "Properties of water-contaminated lubricating oil: Variation with temperature and small water content," *Tribol., Mater., Surf. Interfaces*, vol. 11, no. 1, pp. 1–6, Jan. 2017.

[22] Y. J. Yoon and B. Kim, "A new formula for effective dielectric constant in multi-dielectric layer microstrip structure," in *Proc. IEEE 9th Top. Meeting Electr. Perform. Electron. Packag.*, Oct. 2000, pp. 163–167.

[23] A. Carey. (Jan. 1998). *The Dielectric Constant of Lubrication Oils*. Accessed: Jan. 26, 2023. [Online]. Available: https://apps.dtic.mil/sti/citations/ADA347479

[24] M. Sejkorová, I. Hurtová, P. Jilek, M. Novák, and O. Voltr, "Study of the effect of physicochemical degradation and contamination of motor oils on their lubricity," *Coatings*, vol. 11, no. 1, p. 60, Jan. 2021.

[25] S. L. R. Ellison and A. Williams. (2012). *Quantifying Uncertainty in Analytical Measurement*. Accessed: Apr. 28, 2023. [Online]. Available: https://www.eurachem.org
[26] KERN & SOHN. (2016). *ABT 120-5DNM Technical Datasheet*. Accessed: Apr. 28, 2023. [Online]. Available: https://www.kern-sohn.com
[27] ST Microelectronics. (2020). *STM32F405xx STM32F407xx Datasheet*. Accessed: Apr. 28, 2023. [Online]. Available: https://www.st.com

Antonio Vincenzo Radogna (Member, IEEE) received the M.Eng. degree in electronic engineering from the University of Parma, Parma, Italy, in 2012, and the Ph.D. degree in complex systems engineering from the University of Salento, Lecce, Italy, in 2021.

From 2012 to 2017, he was an Electronic Engineer mainly in the Ambient Assisted Living (AAL) and renewable energies industries. From 2017 to 2023, he was a Research Fellow with the Institute for Microelectronics and Microsystems (IMM), National Research Council (CNR), Lecce. Since 2023, he has been with the Department of Engineering for Innovation, University of Salento, where he is serving as an Assistant Professor. His current research interests include the design of CMOS integrated read-out interfaces for sensors, biomedical electronic circuits for healthcare, *e*-noses development, and agri-food sensing technologies.

Dr. Radogna has been the Team Leader of the NUMINA/CYCLOP business idea, winner of the "Best Research Project" Prize from 2019 to 2020 edition of Contamination Laboratory, University of Salento, and the European "#ConnectingMatters" Prize by EIT Raw Materials.

Chiara De Pascali received the bachelor's degree in information engineering, the master's (Hons.) degree in telecommunication engineering, and the Ph.D. degree in energetic systems and environment from the University of Salento, Lecce, Italy, in 2009 and 2013, respectively.

Since 2013, she has been with the Institute for Microelectronics and Microsystems (IMM), National Research Council (CNR), Lecce. Her research activity is mainly focused on FEM design, fabrication, and characterization of microscale sensors, and MEMS devices for wearable electronics and energy harvesting applications.

Elisa Sciurti was born in Zürich, Switzerland, in 1991. She received the M.Sc. degree in biology from the University of Salento, Lecce, Italy, in 2016, and the joint Ph.D. degree in materials and structural engineering and nanotechnology from the University of Salento and Italian Institute of Technology (IIT-CBN), Lecce, in 2020.

Since 2021, she has been a Post-Doctoral Fellow with the Institute for Microelectronics and Microsystems (IMM), National Research Council (CNR), Lecce. Her research interest focuses on the development of electrochemical sensors for biomedical applications, lab-on-a-chip devices, and energy storage systems.

Maria Assunta Signore received the master's degree in physics from the University of Lecce, Lecce, Italy, in 2002.

In 2004, she joined the National Agency for New Technologies, Energy and Sustainable Economic Development (ENEA), Brindisi, Italy, working in the field of thin film deposition by PVD processes. Since 2010, she has been with the Institute for Microelectronic and Microsystems (IMM), Italian National of Research Council (CNR), Lecce, in Sensors and Microsystems Group, where she has been a permanent Researcher with the National Council of Research, since 2018. She has authored more than 50 peer-reviewed papers in national and international journals. Her research line is mainly dedicated to the field of growth and functional characterization of environmentally sound lead-free piezoelectric materials to integrate into MEMS devices as active layers for a wide range of energy harvesting and sensing applications, including biosensors and implantable sensors. Specifically, piezoelectric thin films, patterned and micromachined by state-of-the-art techniques (i.e., micro/nanolithography and etching) are used for 1) waste-energy harvesting devices with high energy efficiency and 2) sensing solutions responding to aerospace field needs. Suitable technologies have been developed to fabricate piezoelectric thin films working in liquid medium for biosensing applications. She has presented the results of her research, as contributed talk, in more than 20 domestic and international congresses.

Dr. Signore regularly acts as a reviewer for numerous peer-reviewed journals and a member of the examining board for research grants. She has been involved in many national projects, as a component, and as a scientific coordinator.

Stefano D'Amico (Senior Member, IEEE) was born in Lecce, Italy, in 1976. He received the Laurea degree in electronic engineering from the Politecnico di Bari, Bari, Italy, in 2001, and the Ph.D. degree in microelectronics from the Istituto Superiore Universitario per la Formazione Interdisciplinare, (ISUFI), Lecce.

Since 2007, he has been served as an Assistant Professor in Electronics with the Dipartimento di Ingegneria dell-Innovazione, Università del Salento, Lecce, where he has been serving as an Associate Professor, since 2015. In 2015, he co-founded Thetis Microelectronics srls, a startup company operating in the semiconductors field. Since 2002, he has authored or coauthored more than 160 papers in international journals or conference proceedings, seven book chapters, and four international patents. His research interests focus on the design and testing of analog filters, data converters, sensor interfaces, and circuits for power management.

Dr. D'Amico joined the Technical Program Committee of different international conferences: ESSCIRC (since 2016), IEEE ICICDT (since 2012), and IEEE PRIME (since 2012). He was the General Chair of the ICICDT in 2019.

Luca Francioso received the M.Sc. degree in physics from the University of Lecce, Lecce, Italy, in 2001, and the Ph.D. degree from the University of Salento, Lecce, with a thesis on the application of miniaturized gas sensors for combustion and cabin air quality assessment in the automotive field in 2006.

Since 2001, he has been with the Institute for Microelectronic and Microsystems (CNR-IMM), National Research Council, Lecce, working in the field of silicon micromachined systems and solid-state thin-film chemical sensors. Since 2003, he has been a permanent Staff Researcher, devoted to silicon technology development and MEMS device fabrication. He is currently the Head of the Multifunctional Devices Design and Characterization Laboratory (M2DCL), CNR-IMM. He has coauthored many peer-reviewed papers in national and international journals, two book chapters, and several communications to national and international conferences as regular and invited talks. His current research interests are related to: 1) flexible thermoelectric and piezoelectric generators, 2) the design and manufacturing of semiconductor-based chemical sensors, and 3) organ-on-chip platforms.

Open Access funding provided by 'Consiglio Nazionale delle Ricerche-CARI-CARE-ITALY' within the CRUI CARE Agreement